Heuristic Versus Optimal Charging of Supercapacitors, Lithium-Ion, and Lead-Acid Batteries: An Efficiency Point of View

Yasha Parvini, Ardalan Vahidi, and S. Alireza Fayazi

***Abstract*— Electrical energy storage systems are extensively utilized in applications, including electrified vehicles, renewable power generation, and electronic devices. While discharging events are a function of the power demand, the charging procedure is often controllable. This paper evaluates different charging strategies for stand-alone supercapacitors (SCs), lithium-ion (Li-ion), and lead-acid batteries. Constant power and optimal charging strategies are formulated and the corresponding charging currents are obtained. Efficiency analysis for different charging strategies and charging times (slow and fast) is performed. The identical objective function for all modules is to minimize the resistive losses during a given charging time by utilizing Pontryagin's minimum principle. An analytical solution exists for the SC case, which is constant current charging. The variation of the total internal resistance with state of charge in lead-acid chemistry is considerable, and the optimal charging problem results in a two-point boundary value problem. In case of the Li-ion battery, the model includes the electronic as well as polarization resistance. Furthermore, in order to investigate the influence of temperature on the optimal charging of the Li-ion battery, a constrained optimal control problem for a three state electrothermal model is formulated and solved using dynamic programming.**

***Index Terms*— Battery, efficiency, energy storage, fast charging, optimal control, supercapacitor (SC).**

I. Introduction

Batteries have become an indispensable part of our daily life. They can be found almost everywhere from powering our electronic gadgets, computers, and phones to electrifying our vehicles and also form a critical part of the modern centralized and distributed power grids. Supercapacitors (SCs), on the other hand, are the premier energy storage devices in terms of power density, long cycle life, and the ability to operate at extreme temperatures. Much research and development are spurred toward studying important factors influencing the efficiency and cycle life of batteries and SCs, such as monitoring and control of the cell charging method, current rate, number of charging/discharging cycles, and temperature [1]–[10].

Studies that investigate the optimization of efficiency over the entire driving cycle mask the fundamental bottlenecks of efficiency in the electrical energy storage systems. In stand-alone operation and during discharge, the cycle is often imposed by the required load, and therefore, there is little that can be done in reducing resistive losses. During charging, however, there is the opportunity to choose the charging time and profile, such that resistive losses are reduced. Battery manufacturers often have a recommended charging profile, which may be suboptimal.

There are numerous studies focusing on different charging methods to achieve objectives, such as decreasing the charging time [11]–[15], life span [16]–[20], and efficiency maximization or cost minimization. Optimal charging of lithium-ion (Li-ion) batteries is studied in [21], where minimizing the charging time while satisfying specific physical and thermal constraints is considered. In [22], an optimal charging problem is solved for an SC during regenerative braking with the objective of minimizing ohmic losses. Suthar *et al.* [23] use a single-particle model and aim to find the optimal current profile, with the objective of maximizing the charge stored in the cell in a given time and with the constraint of minimal damage to the electrode particles during intercalation. Bashash *et al.* [24] focus on optimizing the timing and charging rate of a plug-in hybrid electric vehicle from the power grid where the goal is to simultaneously minimize the total cost of fuel and electricity and the total battery health degradation. Optimizing the battery charging power in photovoltaic battery systems is studied in [25], where different objectives, such as charging time, battery life time, and cost of charging, are considered. Inoa and Wang [26] suggest optimal charging profiles in order to minimize charging losses and reach a preset temperature at the end of the charging time for Li-ion batteries. More recently, [27] and [28] have solved the optimal charging problem for Li-ion batteries considering the tradeoff between charging time and energy loss in the objective function; however, neither of these papers consider the transient effect of temperature on electrical model parameters of the Li-ion battery. One important output of the mentioned studies is the charging/discharging current profile that satisfies the specific objective functions. For example, there are studies with the objective of reducing the charging time, which

Manuscript received September 29, 2016; accepted December 10, 2016. Date of publication March 6, 2017; date of current version December 14, 2017. Manuscript received in final form February 2, 2017. This work was supported by the Automotive Research Center under Grant W56HZV-04-2-0001 with TARDEC (for technical support). Recommended by Associate Editor M. Guay.

Y. Parvini is with the Department of Mechanical Engineering, University of Detroit Mercy, Detroit, MI 48221 USA (e-mail: parvini@udmercy.edu).

A. Vahidi and S. A. Fayazi are with the Department of Mechanical Engineering, Clemson University, Clemson, SC 29634 USA (e-mail: avahidi@clemson.edu; sfayazi@clemson.edu).

Color versions of one or more of the figures in this paper are available online at http://ieeexplore.ieee.org.

Digital Object Identifier 10.1109/TCST.2017.2665540

result in different types of constant current (CC) charging methods, such as multistage charging [29]–[33], impedance compensation [34]–[36], and pulse charging [37]. Constant voltage (CV) charging has been used to improve charging speed by combining the battery pack and charger models and the results are compared with the CC method [38]. Constant power (CP) charging and discharging are also of interest to researchers as it corresponds to real-world operating conditions, such as in hybrid and electric vehicles. Modeling the thermal behavior of Li-ion batteries under CP charging and discharging cycles is investigated in [39]. Under CP, the relationship between the available energy in a battery and charging power has been investigated in [40]. The aging of SCs under CP charging condition is studied in [41].

The distinctive aspects of this paper compared with the preceding literature are as follows.

1) Our approach isolates the storage system and studies its charging as a component. Unlike system level studies, the charging bottlenecks of the module in this method are clearly identifiable. The significance of this approach is that the results, regardless of the application, are universal.
2) Unlike generic models used in the literature, the model of each module is developed through experimental parameterization in separate studies by the authors and their colleagues. This increases the reliability of the charging profiles and the efficiency analysis.
3) This paper aims to use simple models to break down the problem into cases where the effect of every model parameter on the final result can be identified clearly. This approach also allows to use analytical methods in a number of scenarios. The nature of this paper sets the stage for future studies that attempt to use more complex models.
4) The comparison of almost all charging strategies that are widely used in practice (CV, CC, CP, and CCCV) with their optimal charging scenario counterpart introduces a justifiable framework for choosing the right strategy in a given application. Furthermore, the effect of reduced charging time (fast charging) on the results of the heuristic as well as optimal strategies is investigated.
5) As the most widely used storage technology in transportation and electronic devices, the Li-ion battery is chosen for this paper with a gradual increase in model complexity throughout this paper. The effect of shorter charging times and the resulting increase in temperature, a potential cause of thermal runaway, is investigated in this paper. Discussion on SC charging is included in this paper, which unlike the rich battery literature, is not widely studied.

The common considerations in the problem formulation and analysis for the three SCs, lead-acid, and Li-ion modules are as follows.

1) In all optimal charging formulations, the objective function is to maximize the charging efficiency by minimizing the resistive losses in a given charging time and for a specified range of state of charge (SOC).
2) All problems are formulated using Pontryagin's minimum principle (PMP) method, with the intention to solve them analytically. In cases where analytical solution is not feasible, the problem is solved using numerical methods.
3) The CP and optimal charging current profiles and efficiencies are obtained and compared for all modules.
4) Both slow and fast charging times are investigated.

We begin with lumped models for each module with the upper and lower bounds on SOC being the only constraint considered in the optimal control problem formulations. Later on, we solve the optimal charging problem for the Li-ion battery by coupling a reduced order, two state thermal model to the electrical model in order to investigate the effect of temperature on the optimal result. In the electrical models used in this paper, R_s indicates the ionic and electronic resistance of electrolyte and also the electronic resistance of the electrode. The other two parameters are the charge-transfer resistance R_1, which is in parallel with the double layer capacitance C_1 formed at the interface between the electrode and the electrolyte [42]. In this paper, the sum of R_s and R_1 is called the total internal resistance R. These validated equivalent electric circuit models guarantee the robustness of the model parameters. Also such models facilitate the application of analytical methods that produce results with the highest reliability. However, in order to consider real-world limitations, such as temperature constraints, more complex models, such as the electrothermal model used in this paper, are more suitable. Furthermore, high fidelity electrochemical–thermal models have the capability of clarifying the microscopic bottlenecks in the charging process, such as the lithium plating at high currents and low temperatures. In applications were the charging is performed off-line (i.e., charging an electric vehicle through the outlet) with longer charging times, using simple models, such as the ones in this paper, will be sufficient. In conditions where the goal is to minimize the charging time, the utilization of more complex models is suggested.

In case of the SC, the electrical dynamics is modeled using a constant total internal resistance R. The open circuit voltage (OCV) is assumed to have a linear relationship with SOC. Another assumption is constant ambient temperature of 25 °C during charging. Due to high power density of SCs, the fast and slow charging times are chosen to be 30 s and 6 min, respectively. The optimal charging current and efficiency for the SC have analytical solutions and are compared with the CC and CV strategies. For the lead-acid battery, similar to the SC, the module is modeled using a total constant internal resistance R at a constant ambient temperature of 25 °C. The difference in the problem formulation for the lead-acid battery is the strong dependence of R on SOC, which is integrated into the electrical model. Both OCV and R are approximated by the second-order polynomials as a function of SOC. The fast and slow charging times are chosen to be 6 min and 1 h, respectively. Considering these conditions for the lead-acid battery, the optimal charging formulation results in a two-point boundary value problem (TPBVP), which is solved numerically. The obtained optimal charging current and efficiency are compared with CP and CC methods. For the

TABLE I
SC CELL SPECIFICATION

Nominal Voltage (V)	2.7
Nominal Capacitance (F)	3000
Mass (kg)	0.5
Specific Power (W/kg)	5900
Specific Energy (Wh/kg)	6

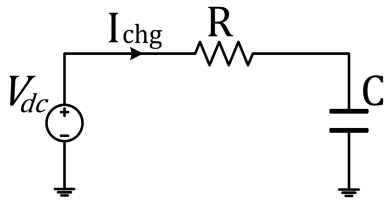

Fig. 1. Schematic of the SC model.

Li-ion battery, in the first step, only the electronic resistance R_s with a constant value at a constant charging temperature of 25 °C is considered. In the second step, the effect of charge-transfer resistance R_1 and double layer capacitance C_1 is added to the model. The dependence of R_s on SOC is negligible at room temperature, and the variation of R_1 and C_1 on SOC has not been considered. Similar to the lead-acid battery, the charging times studied are 6 min and 1 h for rapid and slow charging strategies, respectively. Finally, in order to investigate the effect of temperature on the electrical model parameters, a validated three state electrothermal model is utilized and the optimal charging problem is solved using the numerical method of dynamic programming (DP). The optimal solution in this case is obtained subject to SOC, voltage, and temperature constraints. The unconstrained optimal charging scenarios were partially reported in [22] and [43].

The remainder of this paper is organized in the succeeding order. Section II focuses on the SC, including the model used, CV, CP, optimal charging strategies, and the efficiency analysis. Section III explains the model, charging, and efficiency analysis of the lead-acid battery. Section IV describes the model, charging, and efficiency analysis of the Li-ion battery. Section V presents the electrothermal model and the optimal charging of the Li-ion battery, considering the temperature effect as well as the voltage and temperature constraints. Section VI presents the conclusion remarks.

II. CHARGING OF THE SUPERCAPACITOR

A. Supercapacitor Model and Specifications

The SC utilized in this paper is a Maxwell BCAP3000 cylindrical double layer cell. The specifications of the cell are listed in Table I.

The nominal energy capacity of the SC according to Table I is 3 Wh. The equivalent electric circuit model for this cell is identified using pulse-relaxation experiments for a wide range of temperatures from −40 °C to 60 °C in [44] and [45]. The model indicates that the dependence of the model parameters, such as R in Fig. 1 on SOC and also the current magnitude is negligible. Also as mentioned in Section I, we do not include the thermal constraints in the charging problem formulation and efficiency analysis for the SC. The value of constant electronic resistance R is 2.97 mΩ for this cell at 25 °C. The OCV profile as a function of SOC is assumed to be linear.

B. Constant Voltage Charging of the Supercapacitor

It is well known that charging a capacitor and similarly an SC, from zero charge to full charge, with a CV source results in 50% energy loss, irrespective of the internal and line resistances. This can be easily shown by writing the differential equation governing the SC's stored charge $q(t)$, for the circuit shown in Fig. 1

$$R\,\dot{q} + \frac{q}{C} = V_{\rm dc} \tag{1}$$

where C is the nominal capacitance, R is the total internal resistance, and $V_{\rm dc}$ is the charging voltage. If $V_{\rm dc}$ remains constant over time, the solution to the above-mentioned differential equation from a zero initial charge condition can be obtained as

$$q(t) = CV_{\rm dc}\left[1 - e^{-t/RC}\right] \tag{2}$$

and the CV charging current $I_{\rm chg} = I_{\rm cv}$ is then

$$I_{\rm cv}(t) = \frac{V_{\rm dc}}{R} e^{-t/RC}. \tag{3}$$

The resistive energy loss is obtained by integrating the resistive power loss $RI_{\rm cv}^2$ over the entire charging interval $[0, +\infty)$ as

$$E_{\rm loss,cv} = \frac{V_{\rm dc}^2}{R}\int_0^\infty e^{-2t/RC}dt = \frac{1}{2}CV_{\rm dc}^2. \tag{4}$$

This amount is equal to the total energy stored in the SC. In other words, the efficiency of charging an empty SC with a CV source is 50%, independent of resistance R. Note that the charging efficiency depends on both the initial and final SOC. For example, charging an SC from half to full charge with CV has an efficiency of 75%. Using the definition of efficiency, charging an SC from an initial SOC ($SOC_{\rm i}$) to a final SOC ($SOC_{\rm f}$) with a CV source is

$$\rho_{\rm cv} = \frac{1}{1 + \dfrac{(1 - SOC_{\rm i})^2}{SOC_{\rm f}^2 - SOC_{\rm i}^2}}. \tag{5}$$

C. Constant Power Charging of the Supercapacitor

Consider charging the SC with the model in Fig. 1 by replacing the CV source with a CP source of P_0. Applying Kirchhoff's voltage law to the circuit the stored charge dynamics is

$$R\,\dot{q} + \frac{q}{C} = \frac{P_0}{\dot{q}} \rightarrow \quad \dot{q} = I_{\rm cp} = \frac{-\frac{q}{C} + \sqrt{(\frac{q}{C})^2 + 4RP_0}}{2R} \tag{6}$$

where $I_{\rm cp}$ is the CP charging current. Equation (6), which is a nonlinear differential equation, can be solved numerically to find the charge and current. Consider charging the cell from zero to full charge. Figs. 2 and 3 show the charge stored in

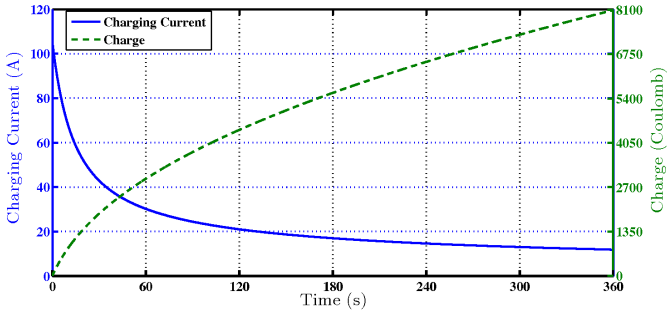

Fig. 2. Charging the SC with CP from zero to full charge in 6 min.

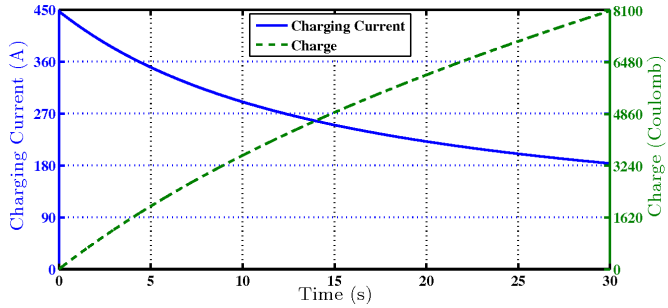

Fig. 3. Charging the SC with CP from zero to full charge in 30 s.

the SC and the CP charging current for charging in 6 min and 30 s, respectively. The maximum storable charge in the SC is $3000 \times 2.7 = 8100$ Coulombs. The CP for charging the cell in 6 min and 30 s is 32 and 595 W, respectively. The maximum current that the cell undergoes in the slow charging (6 min) and fast charging (30 s) is 104.5 and 447.6 A, respectively.

D. Optimal Charging of the Supercapacitor

The next natural question to ask is what charging current profile maximizes the charging efficiency. That is, the current that would charge the SC to a desired level of charge with minimum resistive losses. Let us choose the optimization variable to be the charging current, $u(t) = I_{\text{chg}}(t)$. The SC SOC ($SOC = q(t)/q_{\max}$) quantifies the amount of charge stored in the SC bank normalized by the maximum charge it can accept $q_{\max}$. The dynamics of SOC as the single state x_1 of the problem is derived by coulomb counting using the current $u(t)$, fed into the SC as follows:

$$\frac{d}{dt}x_1(t) = \frac{u(t)}{q_{\max}} = \frac{u(t)}{CV_{\max}} \tag{7}$$

where $V_{\max}$ is the voltage across the cell's terminals at maximum charge and C is the nominal capacitance in farads. Let us assume the SC is initially free of charge $x_1(0) = SOC_{\text{i}} = 0$ and in t_{f} units of time is charged to its final desired SOC SOC_{f}; therefore, $x_1(t_{\text{f}}) = SOC_{\text{f}}$. The optimal input $u(t)$ is one that minimizes the resistive losses in the time period $[0, t_{\text{f}}]$ characterized by the subsequent cost function

$$J = \int_0^{t_{\text{f}}} Ru^2(t)dt. \tag{8}$$

This is an optimal control problem and can be solved using PMP method [46]. First, form the Hamiltonian

$$H(x_1, u, t) = Ru^2(t) + \lambda_1(t)\frac{u(t)}{CV_{\max}} \tag{9}$$

where λ_1 is a costate. The optimal costate should satisfy the subsequent dynamic equation

$$\frac{d}{dt}\lambda_1(t) = -\frac{\partial H}{\partial x_1} = 0 \tag{10}$$

implying that, in this specific problem, the optimal λ_1 must be a constant. The unconstrained optimal solution will also need to satisfy the condition

$$\frac{\partial H}{\partial u} = 0 \rightarrow u(t) = -\frac{1}{2}\frac{1}{RCV_{\max}}\lambda_1(t) \tag{11}$$

showing that the optimal input (charging current) must be a constant. At this point, we can integrate (7) and use the boundary conditions $x_1(0) = SOC_{\text{i}}$ and $x_1(t_{\text{f}}) = SOC_{\text{f}}$ to find the value of this optimal and constant input

$$u_{\text{opt}}(t) = I_{\text{opt,SC}} = \frac{CV_{\max}(SOC_{\text{f}} - SOC_{\text{i}})}{t_{\text{f}}} \tag{12}$$

where the subscript "opt" denotes the optimal solution. This is, in fact, the minimizing solution, since $(\partial^2 H/\partial u^2) > 0$. Given a specific charging time, the most efficient way to charge the SC will be applying a CC equal to (12). The optimal charging current is a CC of 22.5 and 270 A for charging the SC from zero charge to full charge in 6 min and 30 s, respectively.

E. Efficiency Analysis for the Supercapacitor

In order to obtain the charging efficiency of the SC, the total storable energy is required. By the integration of power over the entire charging time and using the definition of SOC, the total energy stored in the SC is obtained as

$$E_{\text{sc}} = \frac{1}{2}CV_{\max}^2\left[SOC_{\text{f}}^2 - SOC_{\text{i}}^2\right]. \tag{13}$$

The energy loss in the SC during optimal charging is already known and is equal to $\int_0^{t_{\text{f}}} Ru_{\text{opt}}^2(t)dt$. Then, the optimal charging efficiency is

$$\rho_{\text{opt}} = \frac{\frac{1}{2}CV_{\max}^2(SOC_{\text{f}}^2 - SOC_{\text{i}}^2)}{\int_0^{t_{\text{f}}} Ru_{\text{opt}}^2(t)dt + \frac{1}{2}CV_{\max}^2(SOC_{\text{f}}^2 - SOC_{\text{i}}^2)}.$$

Substituting for u_{opt} from (12) yields

$$\rho_{\text{opt,SC}} = \frac{1}{1 + (\frac{2RC}{t_{\text{f}}})(\frac{SOC_{\text{f}} - SOC_{\text{i}}}{SOC_{\text{f}} + SOC_{\text{i}}})}. \tag{14}$$

Fig. 4 shows the optimal charging efficiency as a function of initial SOC and (t_{f}/RC) for the SC cell. Fig. 4 implies the expected result that longer charging times and/or smaller RC values improve the charging efficiency. When t_{f} approaches infinity, the charging efficiency approaches 1, which is a 100% improvement over the case with CV charging. Another observation is that beginning the charging from a higher initial SOC and also charging within a narrower range of SOC result in improved efficiency. Furthermore, (14) and the first two profiles that are on top of each other in Fig. 4 show that when starting from zero initial SOC, the charging efficiency

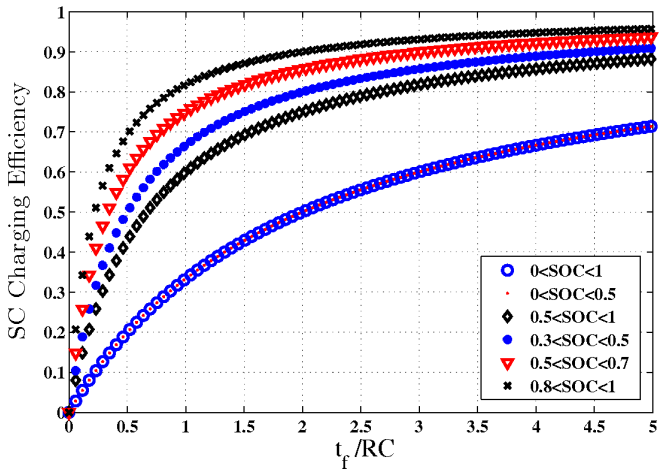

Fig. 4. Effect of charging time, initial SOC, and range of SOC on optimal charging efficiency of the SC.

TABLE II
EFFICIENCY COMPARISON FOR THE SC

		Slow Charging (6 min)		Fast Charging (30 s)		
		CP	Optimal	CP	Optimal	CV
SOC	0-100	93.4	95.28	61.2	62.73	50
	0-50	93.4	95.28	61.2	62.73	20
	50-100	98.32	98.37	83.27	83.47	75

is independent of the final SOC and it is only a function of charging time. The optimal charging current to charge the cell from zero to full charge for slow (6 min) and fast (30 s) charging methods is 22.5 and 270 A, respectively. The maximum allowable peak current of the Maxwell SC cell used in this paper is 2165 A and the maximum allowable continuous current is 147 A. Although, with these upper limits, the fast charging scenario is not practical, it is insightful to compare the corresponding charging currents and efficiencies with the slow charging example. Table II shows the SC charging efficiency for three SOC levels, two charging times, and for CV, CP, and optimal charging strategies. Optimal charging the SC from zero to full charge in 6 min is 1.53% and 45.28% more efficient than CP and CV charging, respectively. The efficiency of charging in the range of 50%–100% SOC (which consists of 75% of the total energy of the SC) is almost equal for CP and CC charging methods. CC is the favorable charging strategy as it is not only more efficient, but also easier to supply than the nonlinear CP charging current.

III. CHARGING OF THE LEAD-ACID BATTERY

A. Lead-Acid Battery Model and Specifications

The lead-acid battery used in this paper is an AP-12220EV-NB module. The module specifications are listed in Table III.

The real capacity of the module is obtained by discharging the fully charged module with a low current of 0.55 A from upper voltage limit to the lower voltage limit. This measured capacity is 19.7 Ah. Specifically designed pulse-relaxation tests, such as the method used in [47], is utilized to estimate the total internal resistance R of the cell as a function of SOC. Fig. 5 shows that the internal resistance of lead-acid battery strongly depends on SOC.

TABLE III
LEAD-ACID MODULE SPECIFICATION

Nominal Voltage (V)	12
Nominal Capacity (Ah)	22
Mass (kg)	6.4
Specific Energy (Wh/kg)	42

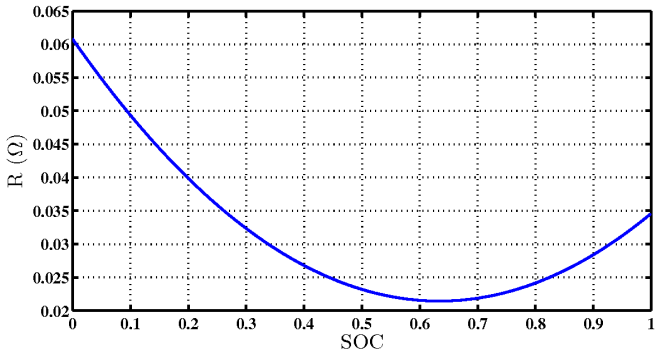

Fig. 5. R versus SOC for the lead-acid battery.

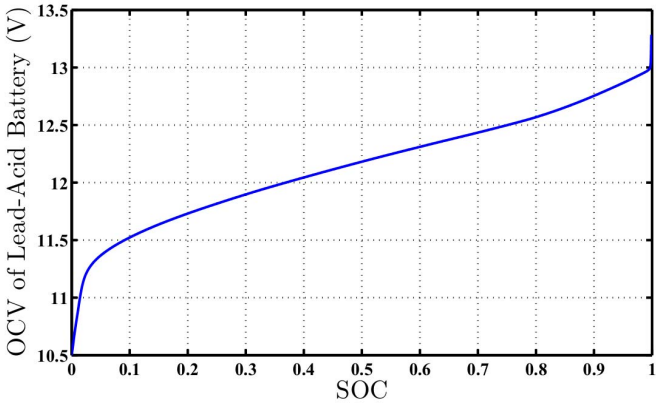

Fig. 6. Measured OCV versus SOC for the lead-acid battery.

The OCV of the lead-acid battery is obtained by applying a small current of 0.05 A to charge the battery from zero to full charge. The recorded OCV for this battery as a function of SOC is shown in Fig. 6.

B. Constant Power Charging of the Lead-Acid Battery

The relationship between the total internal resistance and SOC of the lead-acid battery is approximated by fitting a second-order polynomial to the profile in Fig. 5 as follows:

$$R = a_1 SOC^2 + a_2 SOC + a_3. \tag{15}$$

TABLE IV
POLYNOMIAL COEFFICIENTS FOR THE OCV AND R AS A FUNCTION OF SOC

a_1	a_2	a_3	b_1	b_2	b_3
0.098	-0.12	0.061	-0.56	2.2	11

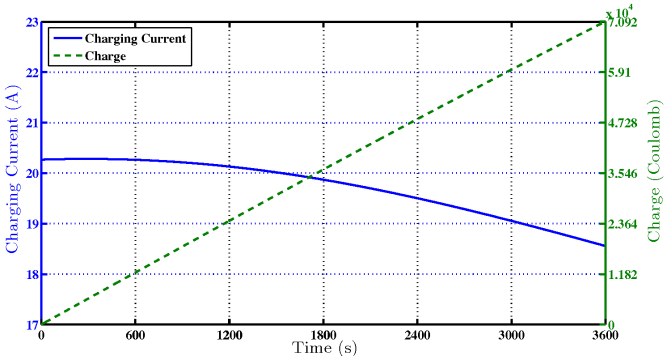

Fig. 7. Charging the lead-acid battery with CP from zero to full charge in 1 h.

A second-order polynomial is fitted to the OCV as a function of SOC profile in Fig. 6 as follows:

$$OCV = b_1 SOC^2 + b_2 SOC + b_3. \tag{16}$$

The polynomial coefficients are listed in Table IV.

As the lead-acid battery is modeled with a total internal resistance of R, applying Kirchhoff's voltage law to the circuit that is charging the lead-acid battery with a CP source (P_0) results in

$$I_{\text{cp}} = \frac{-OCV + \sqrt{OCV^2 + 4RP_0}}{2R}. \tag{17}$$

Substituting (15) and (16) in (17) and solving the nonlinear differential equation, the charge and CP charging current are obtained. Consider charging the empty lead-acid battery to full charge in 1 h where $P_0 = 248\,W$. The maximum charge storable in this lead-acid battery is $19.7\,Ah \times 3600 = 70920$ Coulombs. Fig. 7 shows the charge and CP charging current profiles for charging in 1 h.

For the fast charging case, consider charging the same lead-acid module with a CP of 3660 W, which is equivalent to charging the module in 6 min. Fig. 8 shows that for the lead-acid battery, both the magnitude and shape of the CP charging current vary for the slow and fast charging cases.

C. Optimal Charging of the Lead-Acid Battery

The lead-acid battery is modeled by a single internal resistance in [48], where the only state is the SOC of the battery governed by (7). The objective is to minimize the losses associated with the total internal resistance as in (8). Therefore, the Hamiltonian is

$$H(x, u, t) = R(x_1)u^2(t) + \lambda_2(t)\frac{u(t)}{q_{\max}} \tag{18}$$

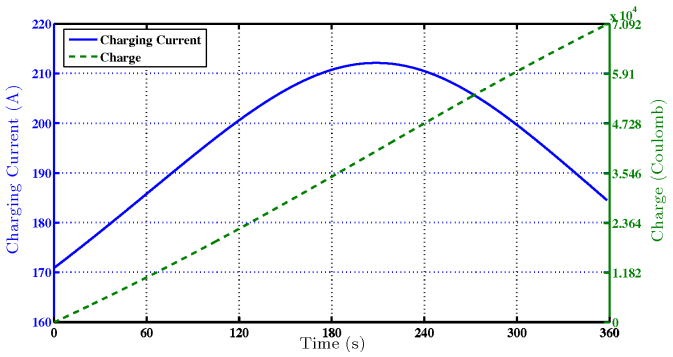

Fig. 8. Charging the lead-acid battery with CP from zero to full charge in 6 min.

where R is the total internal resistance and $\lambda_2(t)$ is the costate. $R(x_1)$ also shown in Fig. 5 is approximated by the second-order polynomial in (15). The necessary conditions to be satisfied are

$$-\frac{\partial H}{\partial x_1} = -\frac{dR(x_1)}{dx_1}u^2(t) = \frac{d}{dt}\lambda_2(t) \tag{19}$$

$$\frac{\partial H}{\partial u} = 2R(x_1)u(t) + \frac{\lambda_2(t)}{q_{\max}} = 0. \tag{20}$$

Solving for $u(t)$ in (20), the optimal charging current is obtained as follows:

$$u_{\text{opt}}(t) = -\frac{1}{2q_{\max}}\frac{1}{R(x_1)}\lambda_2(t). \tag{21}$$

Substituting $u_{\text{opt}}(t)$ from (21) in (7) and (19), the consecutive set of two coupled nonlinear ordinary differential equations (ODEs) are obtained

$$\frac{dx_1(t)}{dt} = -\frac{1}{2q_{\max}^2}\frac{1}{R(x_1)}\lambda_2(t) \tag{22}$$

$$\frac{d\lambda_2(t)}{dt} = -\frac{1}{4q_{\max}^2}\frac{dR(x_1)}{dx_1}\frac{1}{R^2(x_1)}\lambda_2^2(t). \tag{23}$$

Charging the lead-acid battery in t_{f} units of time from zero to full charge requires the initial and final conditions to be satisfied

$$x_1(0) = SOC_{\text{i}}, \quad x_1(t_{\text{f}}) = SOC_{\text{f}}. \tag{24}$$

The system of two nonlinear ODEs with one initial and another final condition forms a TPBVP, which could only be solved using numerical methods. One way to solve this system of ODEs is to specify the initial condition for the SOC and iteratively guess the initial condition for λ_2 until SOC reaches the final specified value. Consider the case of charging the lead-acid battery module from zero to full charge in 1 h. Fig. 9 shows the variation of optimal charging current, SOC, and λ_2 with time.

As shown in the numerical results, the optimal charging current for lead-acid battery, unlike the SC, is not constant. In order to compare the CC charging with the optimal charging strategy, the energy losses in both methods are calculated. For the case of charging the lead-acid battery from zero to full charge in 1 h, the resistive losses in the optimal charging strategy are 46.18 kJ compared with 48.9 kJ for CC charging.

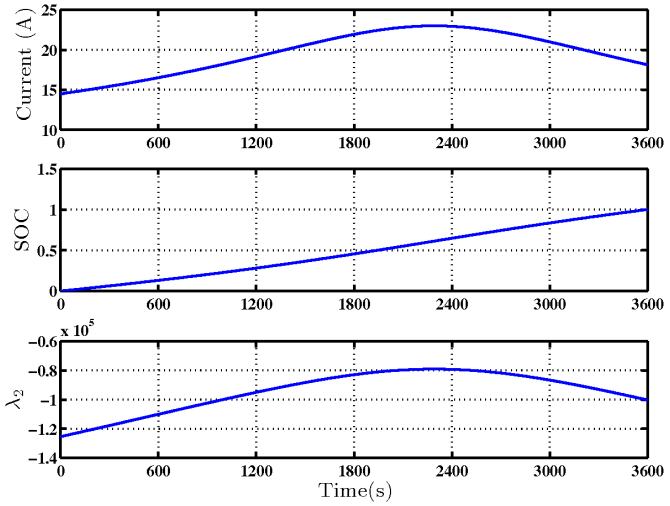

Fig. 9. Optimal charging current, SOC, and λ_2 profiles for charging the lead-acid battery from zero to full charge in 1 h.

TABLE V
EFFICIENCY COMPARISON FOR THE LEAD-ACID BATTERY

Slow Charging (1 h)			Fast Charging (6 min)		
CC	CP	Optimal	CC	CP	Optimal
95.19	95.34	95.44	66.43	67.46	67.70

This is a 5.5% of less energy converted to heat which could be significant in thermal management of battery packs.

D. Efficiency Analysis for the Lead-Acid Battery

The efficiency for three charging strategies including CP, CC, and optimal charging is calculated based on the definition of efficiency

$$\rho = \frac{E_{\text{battery}}}{E_{\text{battery}} + E_{\text{loss}}}. \tag{25}$$

According to the lead-acid battery specification listed in Table III, E_{battery} is 268.8 Wh for this module. The energy loss (E_{loss}) is obtained by numerically integrating the power loss (RI^2) during the charging time. Table V compares the efficiency values for charging the lead-acid battery from zero to full charge for three strategies and two charging times. The efficiency of optimal charging is slightly higher than the other two strategies as expected. If factors, such as cost of supplying a non-CC are considered, one may prefer to charge the lead-acid battery with CC and neglect the effect of the slightly lower charging efficiency. The efficiency of CP charging is higher than CC charging for the lead-acid battery.

IV. CHARGING OF THE LI-ION BATTERY

A. Li-Ion Battery Model and Specifications

The Li-ion battery used in this paper is an A123-26650 cell with $LiFePO_4$ chemistry. The cell specifications are listed in Table VI. The cell model is developed using pulse-relaxation experiments to identify equivalent electric circuit model parameters. The estimation is performed by minimizing the least square error between the experimental and modeled terminal voltages [49].

TABLE VI
LI-ION CELL SPECIFICATION

Nominal Voltage (V)	3.3
Nominal Capacity (Ah)	2.5
Mass (kg)	0.076
Specific Power (W/kg)	2600

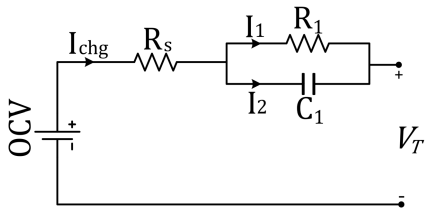

Fig. 10. Schematic of the single RC model for the Li-ion battery.

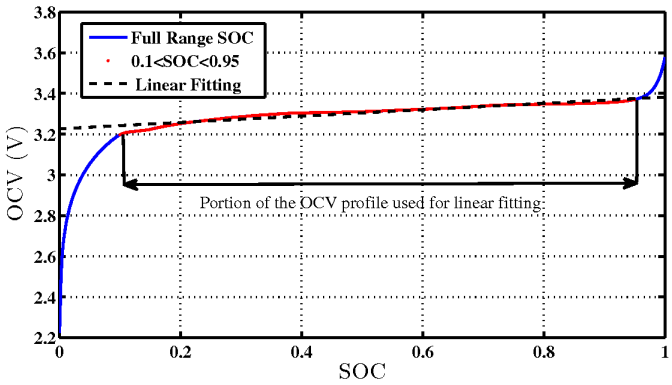

Fig. 11. Actual and approximated OCV versus SOC for the Li-ion battery.

For the Li-ion battery, two models are studied. First, only electronic resistance R_s is considered, and in the next step, the effect of polarization resistance R_1 is also included by adding a single RC branch to the model as shown in Fig. 10. The dependence of model parameters R_s, R_1, and C_1 on SOC can be neglected at room temperature [49]. The values for R_s, R_1, and C_1 are 0.01 Ω, 0.016 Ω, and 2200 F, respectively.

The OCV of the Li-ion battery as a function of SOC is shown in Fig. 11. As shown in Fig. 11, the OCV can be approximated by a linear function using the OCV data in the range of 10%–95% SOC. This linear fit makes the analytical efficiency analysis possible. The linear approximation is governed by

$$OCV(t) = aSOC(t) + b. \tag{26}$$

The relationship between $OCV(t)$ and the charge stored q(t) in the battery is obtained by substituting the definition of

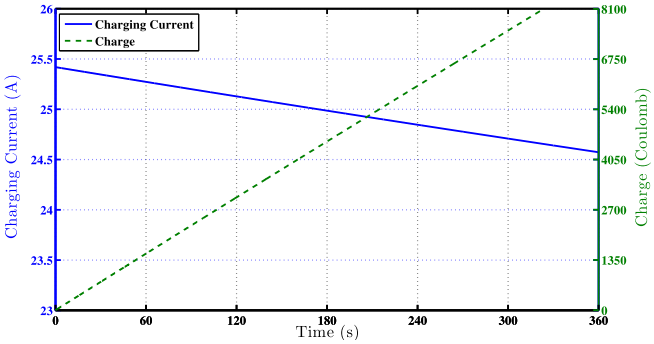

Fig. 12. Charging the Li-ion battery with CP from zero to full charge in 6 min.

SOC in (26) as follows:

$$OCV(t) = \frac{a}{q_{\max}} q(t) + b \tag{27}$$

where a and b for this specific battery are 0.156 and 3.226, respectively.

B. Constant Power Charging of the Li-Ion Battery

Consider charging the Li-ion battery modeled with only the electronic resistance represented with constant R_s in Fig. 10 with a CP source of P_0 and the linear OCV assumption of Fig. 11. Applying Kirchhoff's voltage law to the circuit, the stored charge dynamics is

$$R_s \dot{q} + \left[\frac{a}{q_{\max}} q(t) + b\right] = \frac{P_0}{\dot{q}}. \tag{28}$$

Solving for the CP charging current

$$\dot{q} = I_{cp} = \frac{-\left[\frac{a}{q_{\max}} q(t) + b\right] + \sqrt{\left[\frac{a}{q_{\max}} q(t) + b\right]^2 + 4R_s P_0}}{2R_s}. \tag{29}$$

The nonlinear differential equation in (29) is solved numerically. For the cell used in this paper, the maximum storable charge is $q_{\max} = 2.5\,Ah \times 3600 = 9000$ Coulombs. Fig. 12 shows charge and CP charging current profiles for charging the battery from zero to full charge in 6 min. The CP charging current is linear with small variation during the charging time and a peak amount of 25.4 A. The manufacturer recommends a fast charging of 12 min with a C-rate of 4 (10 A) for this cell. However, in the literature, there are reported Li-ion batteries with nanoparticles of $LiFePO_4$ and $Li_4Ti_5O_{12}$ for the positive and negative electrodes, respectively, which can undergo charging from zero to full charge with C-rates equal to 10 C (6 min) and 15 C (4 min) safely [50].

C. Optimal Charging of the Li-Ion Battery

Two scenarios are considered in the optimal charging of the Li-ion battery. First scenario: in this step, only R_s as shown in Fig. 10 is considered. The value of R_s is constant and equal to 0.01 Ω. The single state is the SOC of the battery x_1, governed by (7). The objective is minimizing the ohmic losses associated with R_s during the given charging time t_f as follows:

$$J_1 = \int_0^{t_f} R_s u^2(t) dt. \tag{30}$$

The optimal charging problem is formulated using the PMP method. The result of the optimal charging strategy in this case is also CC. Similar to the SC case, the value of this optimal charging current for the Li-ion battery is

$$u_{\text{opt}}(t) = I_{\text{opt}} = \frac{q_{\max}(SOC_f - SOC_i)}{t_f}. \tag{31}$$

Similar to the CP case, consider charging the Li-ion battery from zero charge to full charge in 6 min. According to (31), the optimal charging current is constant and equal to 25 A. In this scenario, the CP and optimal charging current profiles are almost identical. Second scenario: in this scenario, the RC branch is added to the model to include the effect of the polarization resistance R_1. The value of R_1 is assumed to be constant and not a function of temperature or SOC. The value for R_1 is 0.016 Ω, which is an average value over the SOC range [49].

Assume I_1 and I_2 are the currents passing through R_1 and C_1, respectively (see Fig. 10). Applying Kirchhoff's current and voltage laws to the RC branch, the second state equation governing the dynamics of I_1 is obtained. The problem, in this case, is to solve for the optimal charging current for a second-order system governed by the state equations as follows:

$$\frac{d}{dt} x_1(t) = \frac{u(t)}{q_{\max}}, \quad \frac{d}{dt} x_2(t) = \frac{1}{R_1 C_1}[u(t) - x_2(t)] \tag{32}$$

where the two states x_1 and x_2 are the SOC of the battery and the current I_1 passing through the polarization resistance R_1. The objective, similar to the first scenario, is to maximize the charging efficiency. The difference is that the contribution of the polarization resistance to the total ohmic losses should also be considered. Therefore, the cost function to be minimized is

$$J_2 = \int_0^{t_f} \left[R_s u^2(t) + R_1 x_2^2(t)\right] dt. \tag{33}$$

The Hamiltonian, in this case, is given by the subsequent equation

$$H(x,u,t) = R_s u(t) + R_1 x_2^2(t) + \lambda_3(t)\frac{u(t)}{q_{\max}} + \frac{\lambda_4(t)}{R_1 C_1}[u(t) - x_2(t)] \tag{34}$$

where λ_3 and λ_4 are the costates. The necessary conditions for optimality are

$$-\frac{\partial H}{\partial x_1} = \frac{d(t)}{dt}\lambda_3, \quad -\frac{\partial H}{\partial x_2} = \frac{d(t)}{dt}\lambda_4, \quad \frac{\partial H}{\partial u} = 0. \tag{35}$$

From the first two conditions in (35), the dynamics of the costates is derived and the solution to the third condition is the optimal input as follows:

$$u_{\text{opt}}(t) = \left[\frac{-1}{2R_s q_{\max}}\right]\lambda_3(t) + \left[\frac{-1}{2} R_s R_1 C_1\right]\lambda_4(t). \tag{36}$$

Substituting the optimal input into the state equations of (32), the optimal state dynamics is derived. The result is a set of four linear first-order ODEs

$$\begin{aligned}
\frac{d}{dt}x_1(t) &= a_1\lambda_3(t) + a_2\lambda_4(t)\\
\frac{d}{dt}x_2(t) &= b_1x_2(t) + b_2\lambda_3(t) + b_3\lambda_4(t)\\
\frac{d}{dt}\lambda_3(t) &= 0\\
\frac{d}{dt}\lambda_4(t) &= c_1x_2(t) + c_2\lambda_4(t)
\end{aligned} \tag{37}$$

where a_1, a_2, b_1, b_2, b_3, c_1, and c_2 are constant parameters equal to

$$\begin{aligned}
a_1 &= \frac{-1}{2R_sq_{max}^2}, \quad a_2 = \frac{-1}{2R_sR_1C_1q_{max}},\\
b_1 &= \frac{-1}{R_1C_1}, \quad b_2 = \frac{-1}{2R_sR_1C_1q_{max}},\\
b_3 &= \frac{-1}{2R_sR_1^2C_1^2}, \quad c_1 = -2R_1, \ c_2 = \frac{1}{R_1C_1}.
\end{aligned} \tag{38}$$

Solving this system of coupled linear ODEs simultaneously results in four algebraic equations with four unknowns. The unknown constants are obtained by applying the boundary conditions specific to this problem, which consist of two initial and two final conditions. The initial and final conditions for $x_1 = SOC$ are similar to (24). On the other hand, in this specific problem, the charging time is specified and fixed while the values of the second state at the initial and final time are free. This results in the succeeding equations for the remaining two boundary conditions [46]

$$\begin{aligned}
&\frac{\partial h}{\partial x_2}(x_2(t_0)) = \lambda_4(t_0) = 0 \rightarrow \text{Initial condition for } x_2\\
&\frac{\partial h}{\partial x_2}(x_2(t_f)) = \lambda_4(t_f) = 0 \rightarrow \text{Final condition for } x_2.
\end{aligned} \tag{39}$$

In general, $h(x(t_f), t_f)$ is the term involving the final states and final time in the cost function, which, in this paper, is zero. Given all boundary conditions, one can solve for the states and costates, and thus, the optimal input is obtained. Consider charging a battery cell from zero charge $SOC_i = x_1(0) = 0$ to full charge $SOC_f = x_1(t_f) = 1$ in 1 h. The result for this example is shown in Fig. 13.

The optimal charging current for this scenario is slightly different from the result of the first scenario. The optimal input in this case is almost a CC equal to 2.5 A, in the majority of times. It may be insightful to also show the result for a fast charging case. Fig. 14 shows the optimal charging current and the two states of the system when the cell is charged from zero to full charge in 6 min.

This charging strategy may not be practical due to thermal and physical constraints plus safety and lifetime issues. However, it may be interesting to observe that by reducing the charging time, the optimal profile differs from the CC result observed in the first scenario and also long charging times in the second scenario.

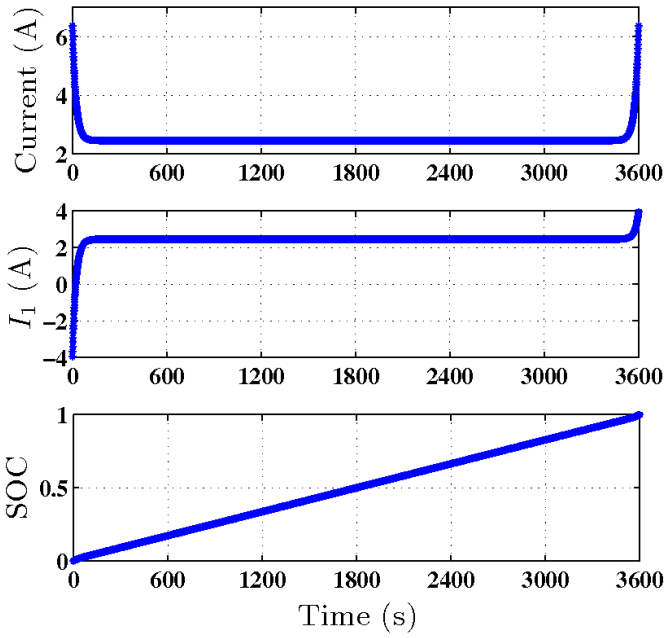

Fig. 13. Optimal charging current, I_1, and SOC for charging the Li-ion battery from zero charge to full charge in 1 h.

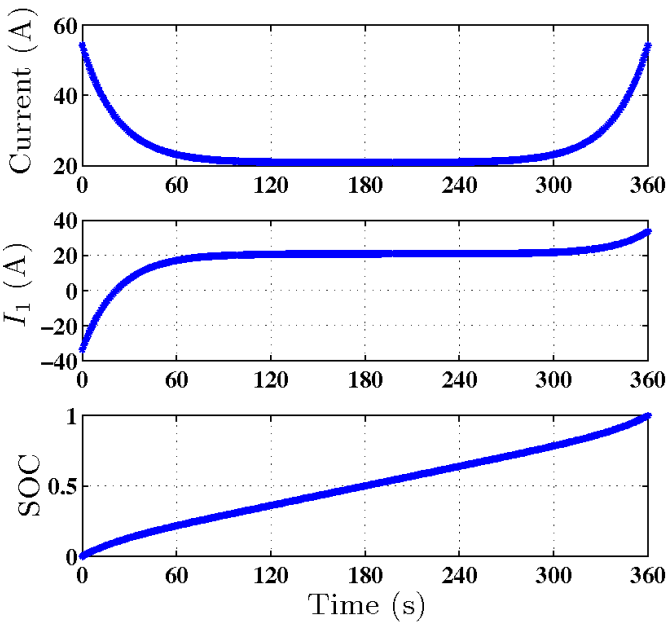

Fig. 14. Optimal charging current, I_1, and SOC for charging the Li-ion battery from zero charge to full charge in 6 min.

D. Efficiency Analysis for the Li-Ion Battery

In order to find the optimal charging efficiency, the total energy stored in the battery and energy loss is required. Assuming a constant total internal resistance ($R = R_s + R_1 = 0.026\,\Omega$) makes the analytical efficiency analysis possible. The energy loss in the battery during optimal charging is already known and is equal to $\int_0^{t_f} Ru_{opt}^2(t)dt$. The total energy stored in the battery is

$$E_{battery} = \int_0^{t_f} VIdt = \int_0^{t_f} V\frac{dq(t)}{dt}dt = \int_{q_i}^{q_f} Vdq \tag{40}$$

where I, V, and q are the battery current, OCV, and the charge in Ah, respectively. Using the linear relationship between OCV and the charge stored in the battery from (27) and the definition of SOC, the maximum energy stored in the battery is obtained as follows:

$$E_{\text{battery}} = q_{\max}(SOC_{\text{f}} - SOC_{\text{i}})\left[\frac{a}{2}(SOC_{\text{f}} + SOC_{\text{i}}) + b\right] \tag{41}$$

where the unit for energy is watt-hour (Wh). The real maximum amount of energy which the battery can store is obtained by integrating the original $(OCV - q)$ profile, which results in 8.2 Wh for the cell used in this paper. Using (41) and charging the battery from 0% to 100%, the maximum battery energy calculated is 8.26 Wh. This illustrates that the linear approximation of OCV for Li-ion battery is an effective approach to perform analytical efficiency analysis. Substituting the expressions for E_{loss} and E_{battery} in (25), the optimal charging efficiency for Li-ion battery is obtained as follows:

$$\rho_{\text{opt}} = \frac{1}{1 + \dfrac{Rq_{\max}(SOC_{\text{f}} - SOC_{\text{i}})}{t_{\text{f}}(\frac{1}{2}a(SOC_{\text{f}} + SOC_{\text{i}}) + b)}} \tag{42}$$

where t_{f} is the charging time in hours and R is the total internal resistance in ohms. Similar to the SC, starting the charging from a higher initial SOC results in better efficiency. Also faster charging will result in higher currents and lower efficiency. For the Li-ion battery, the CP and the two optimal charging scenarios are almost identical in terms of the charging current profiles and also the efficiency values.

V. Effect of Temperature on Optimal Charging of the Li-Ion Battery

In this section, unlike the unconstrained cases solved in Sections II–IV, the optimal problem is solved subject to voltage and temperature constraints. This approach represents a more realistic solution of the optimal charging of the Li-ion battery.

A. Electrothermal Model of the Li-Ion Battery

In order to investigate the effect of temperature on the optimal charging current, a thermal model needs to be coupled with the electrical model and integrated in the optimal charging formulation. The electrical model considered for this section is a single resistance model, which represents the total internal resistance as the sum of the electronic and polarization resistances ($R = R_{\text{s}} + R_1$). The dynamics of the electrical model is governed by the single state equation (7) with current being the input and SOC as the state. On the other hand, the thermal model is a reduced order model represented by two states. For further details on reducing the governing PDE to two linear ODEs, please refer to [51]. The thermal model is identified and validated for the A123-26650 cell with specifications listed in Table VI. The state space representation of the thermal model is

$$\dot{x} = Ax + Bu, \quad y = Cx + Du \tag{43}$$

TABLE VII
Li-Ion Physical and Thermal Parameters

Parameter	Symbol	Value	Unit
Radius	r	12.93e-3	m
Volume	V_{cell}	3.4219e-5	m^3
Density	ρ	2047	$\frac{\text{kg}}{\text{m}^3}$
Specific Heat	c_{p}	1109.2	$\frac{\text{J}}{\text{kgK}}$
Thermal Conductivity	k_{t}	0.61	$\frac{\text{W}}{\text{mK}}$
Convection Coefficient	h	58.6	$\frac{\text{W}}{\text{m}^2\text{K}}$

where $x = [\bar{T}\ \bar{\gamma}]^\top$, $u = [Q\ T_\infty]^\top$, and $y = [T_{\text{c}}\ T_{\text{s}}]^\top$ are state, input, and output vectors, respectively. The states of the thermal model are the volume-averaged temperature $\bar{T}$ in Kelvin (K) and the volume-averaged temperature gradient $\bar{\gamma}$ in (K/m). The inputs are the ambient temperature T_∞ in Kelvin and the total heat generation rate Q. The outputs of the model are the battery's surface temperature T_{s} and core temperature T_{c} both in Kelvin. The linear system matrices A–D are

$$A = \begin{bmatrix} \dfrac{-48\beta h}{r(24k_{\text{t}} + rh)} & \dfrac{-15\beta h}{24k_{\text{t}} + rh} \\ \dfrac{-320\beta h}{r^2(24k_{\text{t}} + rh)} & \dfrac{-120\beta(4k_{\text{t}} + rh)}{r^2(24k_{\text{t}} + rh)} \end{bmatrix}$$

$$B = \begin{bmatrix} \dfrac{\beta}{k_{\text{t}}V_{\text{cell}}} & \dfrac{48\beta h}{r(24k_{\text{t}} + rh)}) \\ 0 & \dfrac{320\beta h}{r^2(24k_{\text{t}} + rh)} \end{bmatrix}$$

$$C = \begin{bmatrix} \dfrac{24k_{\text{t}} - 3rh}{24k_{\text{t}} + rh} & -\dfrac{120rk_{\text{t}} + 15r^2h}{8(24k_{\text{t}} + rh)} \\ \dfrac{24k_{\text{t}}}{24k_{\text{t}} + rh} & \dfrac{15rk_{\text{t}}}{48k_{\text{t}} + 2rh} \end{bmatrix}$$

$$D = \begin{bmatrix} 0 & \dfrac{4rh}{24k_{\text{t}} + rh} \\ 0 & \dfrac{rh}{24k_{\text{t}} + rh} \end{bmatrix}$$

where r, V_{cell}, ρ, c_{p}, k_{t}, and h are radius, volume of the cell, volume-averaged density, specific heat, conduction coefficient, and convective heat transfer coefficients, respectively. The parameter $\beta = (k_{\text{t}})/(\rho c_{\text{p}})$ is the thermal diffusivity. The values for these measured and estimated parameters for the cell used in this paper are summarized in Table VII.

The total heat generation rate obtained from the electrical model is equal to RI^2, which is fed into the thermal model. To complete the coupling and form the electrothermal model, core temperature as an output of the thermal model is fed into the electrical model to tune R. The variation of R with core temperature is estimated by pulse-relaxation experiments at different temperatures ranging from −20 °C (253 K) to 40 °C (313 K) according to [49]. Fig. 15 shows the estimated R as a function of core temperature beside a function fitted to the estimated values, which will be used in the simulations. The fitted function is a sixth-order polynomial

$$R(T_{\text{c}}) = c_1Z^6 + c_2Z^5 + c_3Z^4 + c_4Z^3 + c_5Z^2 + c_6Z + c_7 \quad \text{where } Z = (T_{\text{c}} + d_1)/d_2. \tag{44}$$

The coefficients of the polynomial are listed in Table VIII.

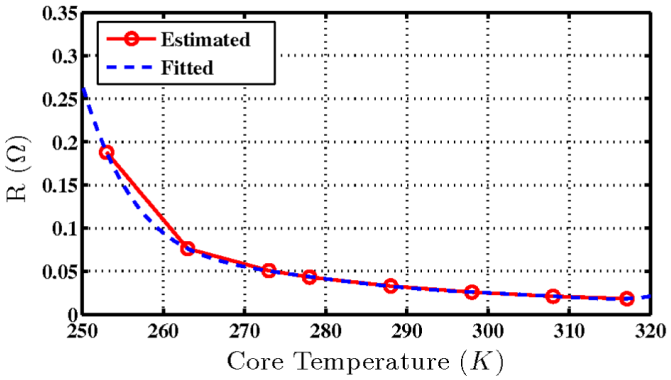

Fig. 15. Internal resistance R as a function of core temperature for the Li-ion battery.

TABLE VIII
POLYNOMIAL COEFFICIENTS FOR R AS A FUNCTION OF T_C

c_1	0.0063599	c_4	0.0071517	c_7	0.035803
c_2	-0.011979	c_5	0.0094349	d_1	-284.77
c_3	-0.0017172	c_6	-0.023463	d_2	22.165

B. Constrained Optimal Fast Charging of the Li-Ion Battery

The described electrothermal model consists of three states. Formulating the efficiency maximization problem using PMP will result in three state equations and three costate dynamic equations with three unknown initial conditions that need to be guessed. This makes the problem tedious to solve using normal nonlinear ODE solvers. DP is used instead to solve this optimal control problem relying on Bellman's principal of optimality. We focus on the optimal charging of the Li-ion battery by realizing that the total internal resistance is a function of core temperature of the cell. The objective similar to the preceding scenarios is to minimize the resistive losses associated with the total internal resistance

$$J = \int_0^{t_f} R(T_c)u^2(t)dt \tag{45}$$

where T_c is the core temperature. Furthermore, we are interested in fast charging while considering the effect of voltage and temperature constraints. For this reason, the charging time of $t_f = 10$ min is chosen. The initial charging temperature is $T_\infty = 25$ °C. The resolution for the time in the DP code is 20 s. At each time instant t_i, all three states of the electrothermal model are quantized and represented by $(SOC_i, \overline{T}_i, \overline{\gamma}_i)$. Fig. 16 demonstrates the implementation of DP. As shown in Fig. 16, each grid represents the three states $(SOC_i, \overline{T}_i, \overline{\gamma}_i)$ moving from time t_{i-1} to t_i with multiple possible transitions. However, only the transitions that satisfy the state equations are acceptable, which are named the admissible transitions in this paper. The first phase of the DP algorithm is solved backward in time. During the backward phase and for every admissible transition, the minimum cost-to-go is obtained for each time instant to the final time along with all the corresponding optimal control inputs. During the forward phase of DP, with the knowledge of initial conditions for the states, the optimal control input, which in this paper is the optimal charging current, is obtained.

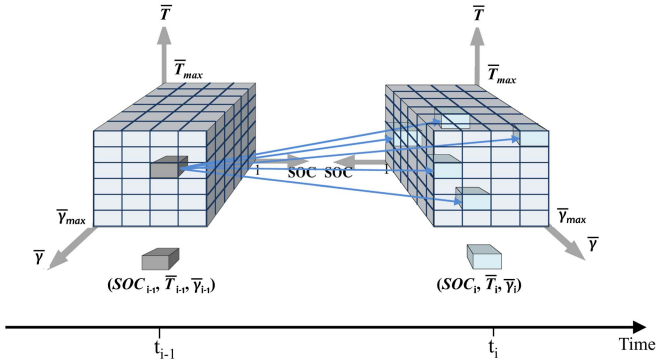

Fig. 16. Illustration of the DP grid and sample transitions.

TABLE IX
UNCONSTRAINED CC AND OPTIMAL CHARGING IN 10 min

	Unconstrained	
	CC	DP
Charging Current (A)	15	20 max.
Core Temperature (°C)	43 max.	42 max.
Terminal Voltage (V)	3.8 max.	3.7 max.
State-of-Charge @t_f	100%	100%
Energy Loss (J)	2682	2638
Efficiency	91.72%	91.84%

CC: Constant Current
DP: Dynamic Programming

Three fast charging scenarios are considered as follows.

1) *Unconstrained Charging:* Similar to the other sections in this paper, the constraints are relaxed and the efficiencies obtained from DP and CC charging are compared for charging from zero to full charge in 10 min. The results are summarized in Table IX where the optimal charging efficiency is slightly higher than CC charging. To be consistent and in order to compare the results with the constrained scenarios, the unconstrained CC and DP charging scenario is resimulated for charging from 0% to 90% which the results are given in the first column of Table X, indicated as CC and DP_1, respectively.
2) *Voltage-Constrained Charging:* A real-world implementation would require constraints on the terminal voltage and core temperature. In the second case, the similar optimal charging problem is solved subject to a voltage constraint given in (46) for both DP and CC charging. In this scenario, the battery is charged from 0% to 90%, since fully charging is not possible due to the voltage constraint as well as the short charging time of 10 min. The results are given in the second column of Table X, indicated as CCCV and DP_2 where CCCV charging is actually the CC charging with the voltage constraint imposed.

TABLE X
CC AND OPTIMAL CHARGING IN 10 MIN CONSIDERING VOLTAGE AND TEMPERATURE CONSTRAINTS

	Unconstrained		Voltage-constrained		Temperature-constrained Voltage-constrained	
	CC	DP_1	CCCV	DP_2	CCCV*	DP_3
Charging Current (A)	13.5	19 max.	13.6 max.	19 max.	20 max.	18 max.
Core Temperature (°C)	41 max.	39 max.	41 max.	40 max.	39 max.	39 max.
Terminal Voltage (V)	3.6 max.	3.7 max.	3.6 max.	3.6 max.	3.6 max.	3.6 max.
State-of-Charge @t_f	90%	90%	90%	90%	90%	90%
Energy Loss (J)	2254	2231	2280	2236	2325	2228
Efficiency	92.95%	93.01%	92.87%	93.00%	92.74%	93.02%

CC: Constant Current
DP: Dynamic Programming
CCCV: Constant Current Constant Voltage
Voltage-constrained: $2\text{V} \leq V_T \leq 3.6\text{V}$
Temperature-constrained: $T_c \leq 39\,^{\circ}\text{C}$

3) *Double Voltage/Temperature Constrained Charging:* In the final scenario, keeping the terminal voltage constraint, the optimal trajectory and efficiency are obtained by adding the core temperature constraint of (47) to both the DP and CC charging methods. Again, the battery is charged from 0% to 90%; and the results are given in the third column of Table X, indicated as CCCV* and DP_3 where CCCV* is the notation for CC charging with both voltage and temperature constraints active

$$2\text{V} \leq V_\text{T} \leq 3.6\text{V} \tag{46}$$

$$T_\text{c} \leq 39\,^{\circ}\text{C}. \tag{47}$$

Neither CC nor DP directly apply a limit on the maximum charging current as the voltage and temperature constraints indirectly result in limited charging current when they become active. The voltage and temperature limits in (46) and (47) are chosen based on the manufacturer's recommendation.

Fig. 17 and the odd columns of Table X present the results for the CC charging. During CCCV charging, as the inset in the first subplot of Fig. 17 shows, the current drops at the end of charging as the terminal voltage hits the limit of 3.6 V. During the CCCV* charging, the amount of initial current (20 A) is chosen, such that the battery could be charged to 90% SOC. According to Fig. 17, at about 30 and 200 s into the CCCV* charging, the voltage and temperature limits are reached, respectively, which results in a stepwise decrease in current. Comparing the efficiencies listed in Table X for CC, CCCV, and CCCV* shows that imposing constraints on the CC charging results in smaller values for efficiency.

Fig. 18 and the even columns of Table X show the results for the optimal charging using DP. As it was mentioned earlier, the unconstrained DP, voltage-constrained, and the double voltage/temperature-constrained problems are indicated as DP_1, DP_2, and DP_3, respectively. The optimal charging has a slightly higher efficiency compared with the CC charging scenarios. The general trajectory of all the three DP cases shows a warm-up period at the beginning of charging followed by a CC charging section. The physical reason behind this behavior is that the higher current at the beginning of charging results in a rapid increase in core temperature, which consequently decreases the total internal resistance. The lower total internal resistance is in favor of minimizing the charging losses according to the objective function in (45). The larger current at the beginning of charging results in terminal voltage reaching the upper limit, which results in a decrease in current for DP_2 and DP_3 scenarios. For DP_3, as also shown via the inset in the second subplot in Fig. 18, the temperature limit is activated toward the end of charging, which results in an instant decrease in current to avoid overheating. The DP results are based on a 20 s resolution on time which maybe the reason for the ripples in current specifically obvious in the DP_2 case.

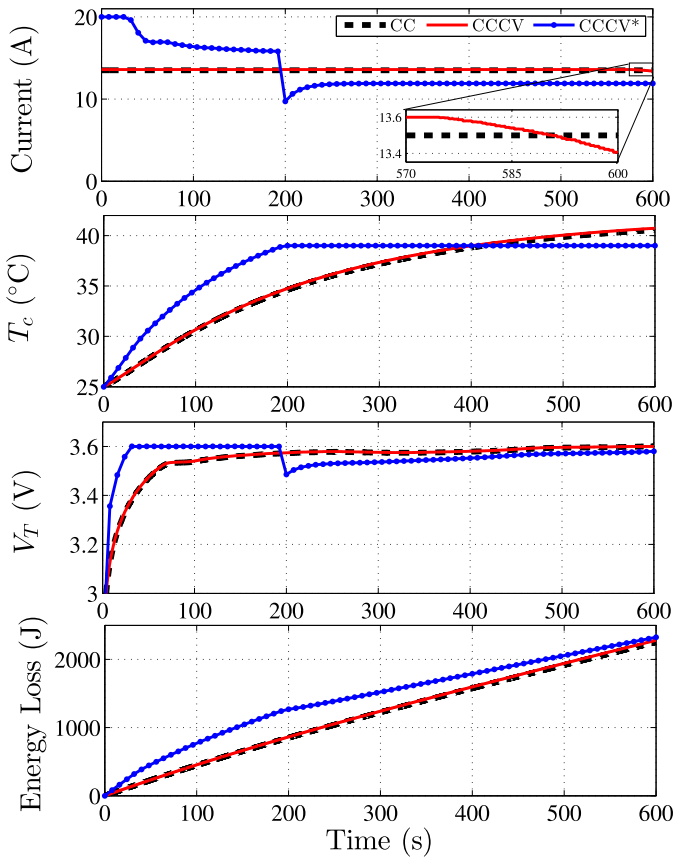

Fig. 17. CC charging results for charging from 0% to 90% in 10 min considering the temperature and voltage constraints.

These optimal solutions are computed using Clemson University's Palmetto cluster to facilitate the high memory requirements of the DP implementation. In this particular problem, the three state variables SOC, $\overline{T}$, and $\overline{\gamma}$ are quantized to $\text{n}_\text{SOC} = 200$, $\text{n}_{\overline{\text{T}}} = 25$, and $\text{n}_{\overline{\gamma}} = 25$, respectively. This requires each grid of Fig. 16 to accommodate $\text{n}_\text{SOC} \times \text{n}_{\overline{\text{T}}} \times \text{n}_{\overline{\gamma}} = 125\,000$ cells. Moreover, each grid is stored by $125\,000 \times 125\,000$ cells in the implementation as each cell at time instant $t_{\text{i-1}}$ has also 125 000 possible transitions to the next cell at time instant t_i. In the implemented DP code, ten variables are involved in the backward DP computation with mixed single/double precision (6 Byte on average). This would mean that the minimum required memory allocation is $10 \times 125\,000 \times 125\,000 \times 6$ Byte or ≈ 870 GB. The involved variables are the two inputs to the objective function ($R(T_\text{c})$ and $u(t)$), three state variables (SOC, $\overline{T}$, $\overline{\gamma}$), one combined constraint based on (46) and (47), and four cost functions.

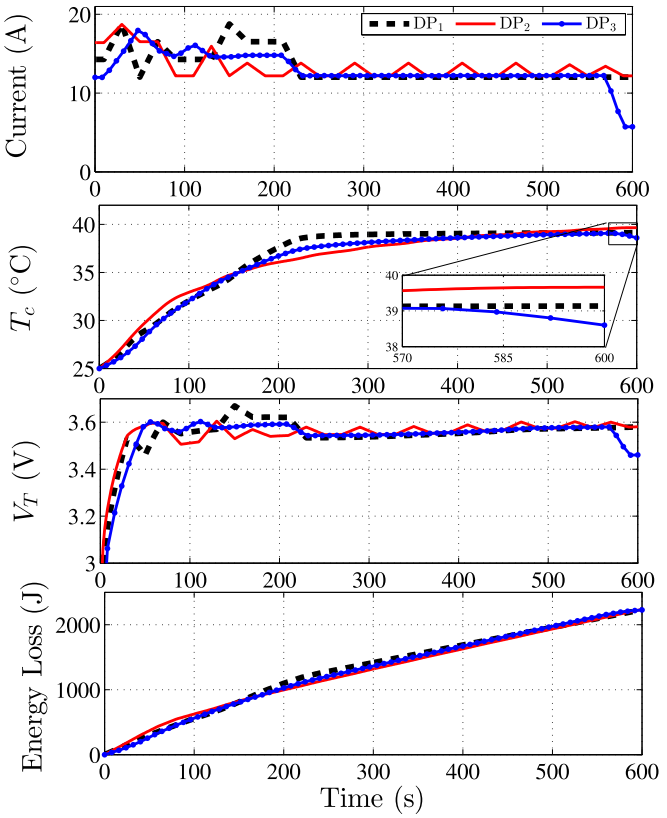

Fig. 18. Optimal charging results via DP for charging from 0% to 90% in 10 min considering the temperature and voltage constraints.

These cost functions include one unconstrained cost-to-go function at $[t_{i\text{-}1}, t_i]$ interval as well as three constrained cost-to-go functions at $[t_{i\text{-}1}, t_i]$, $[t_{i\text{-}1}, t_f]$, and $[t_i, t_f]$ intervals.

VI. Conclusion

This paper solved the optimal charging problem for different energy storage systems considering different levels of model complexity and also compared the optimal charging current with CP, CC, and CV charging strategies. Efficiency analysis was also performed to compare different charging strategies. For the SC and the first scenario of the Li-ion battery, the optimal charging strategy is CC. In the SC case, the CP charging current has peaks that may make it less favorable to apply, as it is also less efficient. In the Li-ion case, there is not much difference in applying CP or CC considering the efficiency and shape of the current profile. For the lead-acid battery, the optimal strategy has a better efficiency than CP charging, while CC charging has the least efficiency. Finally, the effect of temperature dependent model parameters as well as the voltage and temperature constraints on the optimal fast charging of the Li-ion battery was investigated. This constrained optimal control problem was solved using DP and was compared with CC charging. The results show that the charging efficiency of the optimal scenario is slightly higher than CC charging.

References

[1] M. Fleischhammer, T. Waldmann, G. Bisle, B.-I. Hogg, and M. Wohlfahrt-Mehrens, "Interaction of cyclic ageing at high-rate and low temperatures and safety in lithium-ion batteries," *J. Power Sour.*, vol. 274, pp. 432–439, Jan. 2015.

[2] J. Groot, M. Swierczynski, A. I. Stan, and S. K. Kær, "On the complex ageing characteristics of high-power $LiFePO_4$/graphite battery cells cycled with high charge and discharge currents," *J. Power Sour.*, vol. 286, pp. 475–487, Jul. 2015.

[3] B. Suthar, P. W. Northrop, R. D. Braatz, and V. R. Subramanian, "Optimal charging profiles with minimal intercalation-induced stresses for lithium-ion batteries using reformulated pseudo 2-dimensional models," *J. Electrochem. Soc.*, vol. 161, no. 11, pp. F3144–F3155, 2014.

[4] A. Barré, B. Deguilhem, S. Grolleau, M. Gérard, F. Suard, and D. Riu, "A review on lithium-ion battery ageing mechanisms and estimations for automotive applications," *J. Power Sour.*, vol. 241, pp. 680–689, Nov. 2013.

[5] Y. Zhang, W. Song, and Z. Feng, "An energy efficiency evaluation research based on heat generation behavior of lithium-ion battery," *J. Electrochem. Soc.*, vol. 160, no. 11, pp. A1927–A1930, 2013.

[6] R. Kötz, M. Hahn, and R. Gallay, "Temperature behavior and impedance fundamentals of supercapacitors," *J. Power Sour.*, vol. 154, no. 2, pp. 550–555, 2006.

[7] O. Bohlen, J. Kowal, and D. U. Sauer, "Ageing behaviour of electrochemical double layer capacitors: Part I. Experimental study and ageing model," *J. Power Sour.*, vol. 172, no. 1, pp. 468–475, 2007.

[8] M. Uno and K. Tanaka, "Accelerated charge–discharge cycling test and cycle life prediction model for supercapacitors in alternative battery applications," *IEEE Trans. Ind. Electron.*, vol. 59, no. 12, pp. 4704–4712, Dec. 2012.

[9] V. Svoboda, H. Doering, and J. Garche, "The influence of fast charging on the performance of VRLA batteries," *J. Power Sour.*, vol. 144, no. 1, pp. 244–254, 2005.

[10] D. Pavlov, G. Petkova, M. Dimitrov, M. Shiomi, and M. Tsubota, "Influence of fast charge on the life cycle of positive lead–acid battery plates," *J. Power Sour.*, vol. 87, no. 1, pp. 39–56, 2000.

[11] S. K. Rahimian, S. C. Rayman, and R. E. White, "Maximizing the life of a lithium-ion cell by optimization of charging rates," *J. Electrochem. Soc.*, vol. 157, no. 12, pp. A1302–A1308, 2010.

[12] P. H. L. Notten, J. H. G. Op het Veld, and J. R. G. van Beek, "Boostcharging Li-ion batteries: A challenging new charging concept," *J. Power Sour.*, vol. 145, no. 1, pp. 89–94, 2005.

[13] I. A. Hamad, M. Novotny, D. Wipf, and P. Rikvold, "A new battery-charging method suggested by molecular dynamics simulations," *Phys. Chem. Chem. Phys.*, vol. 12, no. 11, pp. 2740–2743, 2010.

[14] S. J. Moura, N. A. Chaturvedi, and M. Krstić, "Constraint management in Li-ion batteries: A modified reference governor approach," in *Proc. Amer. Control Conf.*, Jun. 2013, pp. 5332–5337.

[15] M. Torchio *et al.*, "Real-time model predictive control for the optimal charging of a lithium-ion battery," in *Proc. Amer. Control Conf.*, Jul. 2015, pp. 4536–4541.

[16] P. Keil and A. Jossen, "Charging protocols for lithium-ion batteries and their impact on cycle life—An experimental study with different 18650 high-power cells," *J. Energy Storage*, vol. 6, pp. 125–141, May 2016.

[17] D. Anseán *et al.*, "Fast charging technique for high power $LiFePO_4$ batteries: A mechanistic analysis of aging," *J. Power Sour.*, vol. 321, pp. 201–209, Jul. 2016.

[18] M. A. Monem *et al.*, "Lithium-ion batteries: Evaluation study of different charging methodologies based on aging process," *Appl. Energy*, vol. 152, pp. 143–155, Aug. 2015.

[19] B. Lunz, Z. Yan, J. B. Gerschler, and D. U. Sauer, "Influence of plug-in hybrid electric vehicle charging strategies on charging and battery degradation costs," *Energy Policy*, vol. 46, pp. 511–519, Jul. 2012.

[20] Z. Guo, B. Y. Liaw, X. Qiu, L. Gao, and C. Zhang, "Optimal charging method for lithium ion batteries using a universal voltage protocol accommodating aging," *J. Power Sour.*, vol. 274, pp. 957–964, Jan. 2015.

[21] R. Klein, N. Chaturvedi, J. Christensen, J. Ahmed, R. Findeisen, and A. Kojic, "Optimal charging strategies in lithium-ion battery," in *Proc. Amer. Control Conf.*, Jun. 2011, pp. 382–387.

[22] Y. Parvini and A. Vahidi, "Optimal charging of ultracapacitors during regenerative braking," in *Proc. IEEE Int. Elect. Veh. Conf.*, Mar. 2012, pp. 1–6.

[23] B. Suthar, V. Ramadesigan, S. De, R. D. Braatz, and V. R. Subramanian, "Optimal charging profiles for mechanically constrained lithium-ion batteries," *Phys. Chem. Chem. Phys.*, vol. 16, no. 1, pp. 277–287, 2013.

[24] S. Bashash, S. J. Moura, J. C. Forman, and H. K. Fathy, "Plug-in hybrid electric vehicle charge pattern optimization for energy cost and battery longevity," *J. Power Sour.*, vol. 196, no. 1, pp. 541–549, Jan. 2011.

[25] J. Li and M. A. Danzer, "Optimal charge control strategies for stationary photovoltaic battery systems," *J. Power Sour.*, vol. 258, pp. 365–373, Jul. 2014.

[26] E. Inoa and J. Wang, "PHEV charging strategies for maximized energy saving," *IEEE Trans. Veh. Technol*, vol. 60, no. 7, pp. 2978–2986, Sep. 2011.
[27] X. Hu, S. E. Li, H. Peng, and F. Sun, "Charging time and loss optimization for LiNMC and $LiFePO_4$ batteries based on equivalent circuit models," *J. Power Sour.*, vol. 239, pp. 449–457, Oct. 2013.
[28] A. Abdollahi *et al.*, "Optimal battery charging, Part I: Minimizing time-to-charge, energy loss, and temperature rise for OCV-resistance battery model," *J. Power Sour.*, vol. 303, pp. 388–398, Jan. 2016.
[29] T. T. Vo, X. Chen, W. Shen, and A. Kapoor, "New charging strategy for lithium-ion batteries based on the integration of Taguchi method and state of charge estimation," *J. Power Sour.*, vol. 273, pp. 413–422, Jan. 2015.
[30] Y.-H. Liu and Y.-F. Luo, "Search for an optimal rapid-charging pattern for Li-ion batteries using the Taguchi approach," *IEEE Trans. Ind. Electron.*, vol. 57, no. 12, pp. 3963–3971, Dec. 2010.
[31] Y.-H. Liu, C.-H. Hsieh, and Y.-F. Luo, "Search for an optimal five-step charging pattern for Li-ion batteries using consecutive orthogonal arrays," *IEEE Trans. Energy Convers.*, vol. 26, no. 2, pp. 654–661, Jun. 2011.
[32] Y.-H. Liu, J.-H. Teng, and Y.-C. Lin, "Search for an optimal rapid charging pattern for lithium-ion batteries using ant colony system algorithm," *IEEE Trans. Ind. Electron.*, vol. 52, no. 5, pp. 1328–1336, Oct. 2005.
[33] S. S. Zhang, "The effect of the charging protocol on the cycle life of a Li-ion battery," *J. Power Sour.*, vol. 161, no. 2, pp. 1385–1391, 2006.
[34] L. R. Chen, R. C. Hsu, and C. S. Liu, "A design of a grey-predicted Li-Ion battery charge system," *IEEE Trans. Ind. Electron.*, vol. 55, no. 10, pp. 3692–3701, Oct. 2008.
[35] C. H. Lin, C. Y. Hsieh, and K. H. Chen, "A Li-Ion battery charger with smooth control circuit and built-in resistance compensator for achieving stable and fast charging," *IEEE Trans. Circuits Syst. I, Reg. Papers*, vol. 57, no. 2, pp. 506–517, Feb. 2010.
[36] L. R. Chen, C. S. Liu, and J. J. Chen, "Improving phase-locked battery charger speed by using resistance-compensated technique," *IEEE Trans. Ind. Electron.*, vol. 56, no. 4, pp. 1205–1211, Apr. 2009.
[37] L. R. Chen, "A design of an optimal battery pulse charge system by frequency-varied technique," *IEEE Trans. Ind. Electron.*, vol. 54, no. 1, pp. 398–405, Feb. 2007.
[38] Y.-D. Lee and S.-Y. Park, "Rapid charging strategy in the constant voltage mode for a high power Li-Ion battery," in *Proc. Energy Convers. Congr. Expo.*, Sep. 2013, pp. 4725–4731.
[39] U. S. Kim, J. Yi, C. B. Shin, T. Han, and S. Park, "Modeling the thermal behaviors of a lithium-ion battery during constant-power discharge and charge operations," *J. Electrochem. Soc.*, vol. 160, no. 6, pp. A990–A995, 2013.
[40] E. M. Krieger and C. B. Arnold, "Effects of undercharge and internal loss on the rate dependence of battery charge storage efficiency," *J. Power Sour.*, vol. 210, pp. 286–291, Jul. 2012.
[41] K. Paul, M. Christian, V. Pascal, C. Guy, R. Gerard, and Z. Younes, "Constant power cycling for accelerated ageing of supercapacitors," in *Proc. 13th Eur. Conf. Power Electron. Appl. (EPE)*, Sep. 2009, pp. 1–10.
[42] S. Sato and A. Kawamura, "A new estimation method of state of charge using terminal voltage and internal resistance for lead acid battery," in *Proc. Power. Convers. Conf.*, vol. 2. Apr. 2002, pp. 565–570.
[43] Y. Parvini and A. Vahidi, "Maximizing charging efficiency of lithium-ion and lead-acid batteries using optimal control theory," in *Proc. Amer. Control Conf.*, Jul. 2015, pp. 317–322.
[44] Y. Parvini, J. B. Siegel, A. G. Stefanopoulou, and A. Vahidi, "Supercapacitor electrical and thermal modeling, identification, and validation for a wide range of temperature and power applications," *IEEE Trans. Ind. Electron.*, vol. 63, no. 3, pp. 1574–1585, Mar. 2016.
[45] Y. Parvini, J. B. Siegel, A. G. Stefanopoulou, and A. Vahidi, "Preliminary results on identification of an electro-thermal model for low temperature and high power operation of cylindrical double layer ultracapacitors," in *Proc. Amer. Control Conf.*, Jun. 2014, pp. 242–247.
[46] D. Kirk, *Optimal Control Theory: An Introduction*. Mineola, NY, USA: Dover, 2004.
[47] S. Fiorenti, J. Guanetti, Y. Guezennec, and S. Onori, "Modeling and experimental validation of a hybridized energy storage system for automotive applications," *J. Power Sour.*, vol. 241, pp. 112–120, Nov. 2013.
[48] Y. Parvini, "Modeling, hybridization, and optimal charging of electrical energy storage systems," Ph.D. dissertation, Dept. Mech. Eng., Clemson Univ., Clemson, SC, USA, Aug. 2016.
[49] X. Lin *et al.*, "A lumped-parameter electro-thermal model for cylindrical batteries," *J. Power Sour.*, vol. 257, pp. 1–11, Jul. 2014.
[50] K. Zaghib *et al.*, "Safe and fast-charging Li-ion battery with long shelf life for power applications," *J. Power Sour.*, vol. 196, no. 8, pp. 3949–3954, 2011.
[51] Y. Kim, S. Mohan, J. B. Siegel, A. G. Stefanopoulou, and Y. Ding, "The estimation of temperature distribution in cylindrical battery cells under unknown cooling conditions," *IEEE Trans. Control Syst. Technol.*, vol. 22, no. 6, pp. 2277–2286, Nov. 2014.

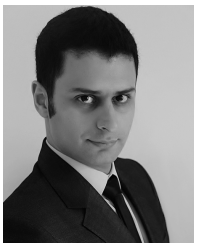

Yasha Parvini received the B.Sc. degree in mechanical engineering from the University of Tabriz, Tabriz, Iran, the M.Sc. degree in mechanical engineering from Sharif University of Technology, Tehran, Iran, and the Ph.D. degree in mechanical engineering from Clemson University, Clemson, SC, USA, in 2016.

He was a Visiting Researcher with the University of Michigan, Ann Arbor, MI, USA, from 2012 to 2013. He is currently an Assistant Professor of Mechanical Engineering at the University of Detroit Mercy, Detroit, MI, USA. His current research interests include the modeling, estimation, and control of electrical energy storage systems, such as batteries and supercapacitors in mobile and stationary applications.

Ardalan Vahidi received the B.S. and M.Sc. degrees in civil engineering from Sharif University, Tehran, Iran, in 1996 and 1998, respectively, the M.Sc. degree in transportation safety from George Washington University, Washington, DC, USA, in 2002, and the Ph.D. degree in mechanical engineering from the University of Michigan, Ann Arbor, MI, USA, in 2005.

He has been a Visiting Scholar with the University of California at Berkeley, Berkeley, CA, USA, and a Visiting Researcher with BMW Group Technology Office, Mountain View, CA, USA, from 2012 to 2013. He is currently an Associate Professor with the Department of Mechanical Engineering, Clemson University, Clemson, SC, USA. His current research interests include the control of vehicular and energy systems, and connected vehicle technologies.

S. Alireza Fayazi received the B.Sc. degree in electrical and electronics engineering from the K. N. Toosi University of Technology, Tehran, Iran, the M.Sc. degree from the University of Tehran, Tehran, and the Ph.D. degree in systems and controls from Clemson University, Clemson, SC, USA.

From 2012 to 2013, he was a Visiting Researcher with the University of California at Berkeley, Berkeley, CA, USA, and was also a Visiting Researcher with the BMW Group Technology Office, Mountain View, CA, USA. He was a Research and Development Engineer with Kerman Tablo Corporation, Kerman, Iran, for three years where he was involved in discrete control systems and digital control for embedded applications. He is currently a Research Specialist with Clemson University.